

Report of Visiting Scientist mission NWP_VS16_01

Document NWPSAF-MO-VS-054

Version 1.0

28-06-16

A comparison of MFASIS and RTTOV-DOM

Leonhard Scheck¹, James Hocking², and Roger Saunders²

1 Ludwig-Maximilians-University, Munich, Germany

2 Met Office, Exeter, UK

The EUMETSAT Network of Satellite Application Facilities	 NWP SAF Numerical Weather Prediction	A comparison of MFASIS and RTTOV-DOM	Doc ID : NWP-MO-VS-054 Version : 1.0 Date : 28/6/16
---	--	---	---

A comparison of MFASIS and RTTOV-DOM

Leonhard Scheck (LMU),
James Hocking and Roger Saunders (Met Office)

This documentation was developed within the context of the EUMETSAT Satellite Application Facility on Numerical Weather Prediction (NWP SAF), under the Cooperation Agreement dated 29 June 2011, between EUMETSAT and the Met Office, UK, by one or more partners within the NWP SAF. The partners in the NWP SAF are the Met Office, ECMWF, KNMI and Météo France.

Copyright 2016, EUMETSAT, All Rights Reserved.

Change record			
Version	Date	Author / changed by	Remarks
0.1	17/6/16	Leonhard Scheck	Draft version
0.2	27/6/16	Roger Saunders/ James Hocking	Some revisions
1.0	28/6/16	Leonhard Scheck	Final version

A Comparison of MFASIS and RTTOV-DOM

Leonhard Scheck

Hans-Ertel Center for Weather Research, Ludwig-Maximilians-University, Munich, Germany

James Hocking, Roger Saunders

MetOffice, Exeter, UK

Abstract

Two methods to generate synthetic satellite images in the visible spectrum from data generated by numerical weather prediction models are compared: the implementation of the discrete ordinate method in RTTOV and the look-up table based method MFASIS, which is several orders of magnitude faster. It is shown that after compensating for different assumptions about the input parameters both methods give very similar results for water and ice clouds. Some differences are found when the cloud-free atmosphere is included. Not all multiple scattering processes involving clouds and air molecules are accounted for in RTTOV, which leads to too low reflectances for bright clouds. In MFASIS the spatial variation of water vapour is neglected, which causes some error in channels containing water vapour bands. The different deterministic and stochastic approaches to account for cloud overlap implemented in the two methods (including a potentially more efficient variant of the streams method) lead to similar results. MFASIS can be used as a fast emulator of RTTOV-DOM and could be included in RTTOV without changing the application programming interface.

1 Introduction

Visible satellite images provide a wealth of information about the spatial distribution and the microphysical properties of clouds. The assimilation of this information requires fast and accurate forward operators. The importance of multiple scattering in the solar spectrum makes radiative transfer more complex and computationally more expensive than in the thermal spectrum. Consequently, standard radiative transfer (RT) methods for visible wavelengths tend to be too slow or too inaccurate for operational purposes. A new look-up table (LUT) based method developed at LMU Munich, MFASIS (method for fast satellite image synthesis) generates sufficiently accurate results orders of magnitude faster than standard methods like the discrete ordinate method (DOM). The reflectance LUT used by MFASIS was generated by an implementation of DOM that is part of the libRadtran package.

The primary goal of the visiting scientist mission was to compare MFASIS to an implementation of DOM developed within RTTOV, which we will refer to as RTTOV-DOM. A second goal of the mission was to investigate if changes in the RTTOV interface would be required to integrate methods like MFASIS into RTTOV. Finally, the third goal was to demonstrate that a MFASIS LUT can actually be used as an fast emulator for RTTOV-DOM by generating an MFASIS LUT using RTTOV-DOM.

The rest of this report is organized as follows: Section 2 contains a short description of the methods and the data used for comparisons. In Sect. 3 differences in the input parameters are discussed. Differences in the radiative transfer processes are described in 4. The topic of Sect. 5 are results based on a RTTOV-generated MFASIS LUT. Section 6 contains a

discussion of how MFASIS could be integrated into RTTOV and in Sect. 7 we summarize our results.

2 Methods and data

RTTOV-DOM is an implementation of the discrete ordinates method (DOM) originally developed by Chandrasekhar (1960) and significantly improved by Stamnes, K. et al. (1988). At the moment RTTOV-DOM is still in development. It will be included in one of the next releases of RTTOV. For all results in this report 8 DOM streams (i.e. angular directions) were used. Several computations were repeated with 32 streams and showed little differences.

MFASIS (Scheck et al., 2016) is a look-up table (LUT) based method to generate synthetic satellite images from model data. It relies on the fact that for a given total (vertically integrated) optical depth the vertical cloud structure has only a very weak influence on the reflectance. Therefore, 8 parameters are sufficient to characterize the radiative transfer problem: the total water and ice cloud optical depths, water and ice effective particle sizes, the surface albedo and three angles defining the sun and satellite geometry. Using the scattering angle as one of the table dimensions allows for an efficient compression of the LUT that would otherwise be tens of gigabytes in size. The MFASIS LUT was generated using the DOM implementation in the radiative transfer package libRadtran (Mayer, B. and Kylling, A., 2005; Emde et al., 2016). The reflectance LUT is computed for fixed profiles of water vapour and trace gas concentrations. In contrast, DOM itself is more flexible and allows for arbitrary profiles in each pixel. The advantage of MFASIS is that it is four orders of magnitude faster than the DOM implementation in libRadtran (Scheck et al., 2016)¹.

VISOP is a python script that converts the output of NWP models like COSMO into the input variables required by radiative transfer codes, taking also subgrid clouds into account. Moreover, it performs a parallax correction to account for slant viewing angles and manages the parallel execution of the RT codes. VISOP supports MFASIS and the DOM implementation from libRadtran. In the course of the visiting scientist mission RTTOV-DOM was added as a further option.

For the generation of the MFASIS LUT idealized cloud scenes with a homogeneous water cloud between 2km and 4km height and a homogeneous ice cloud between 6km and 8km height embedded in the US standard summer atmosphere provided with libRadtran were used. These scenes – with varying parameters for the cloud optical thickness, effective particle sizes, viewing and sun angles – were also used to compare RTTOV-DOM and MFASIS. In addition, synthetic SEVIRI satellite images computed from operational COSMO-DE (Baldauf et al., 2011) forecasts performed by the german weather service for a test period in June 2012 (the same period as in used in Scheck et al., 2016) using RTTOV-DOM and MFASIS were compared.

3 Differences in the input parameters

3.1 Input parameters RTTOV-DOM

For the computation of reflectances for visible satellite channels RTTOV-DOM requires vertical profiles of LWC , IWC , water vapour, pressure, temperature, cloud type, effective ice particle diameter as well as values for the albedo, the sun and satellite angles. Various other parameters can be specified, which should not have a significant influence on visible satellite

¹For only one cloud stream (no partially cloudy layers) and not taking into account the time required to compute optical properties.

channels but are important for other applications. The cloud type parameter documented in Matricardi (2005) determines several other important parameters. By selecting one of 5 clouds types (see Tab. 1) the effective droplet radius, the shape of the droplet size distribution (see Fig. 1a) and the way the optical depth is computed from the water content are chosen. According to Hu and Stamnes (1993) the radiative properties of a water cloud depend for optical thickness mainly on the effective droplet radius

$$r_{\text{eff,w}} = \frac{\int_0^\infty r^3 n(r) dr}{\int_0^\infty r^2 n(r) dr} \quad (1)$$

and are insensitive to details of the size distribution function $n(r)$. RTTOV assumes a linear relationship between LWC and the droplet concentration N ,

$$N = \frac{N_0^{(k)}}{LWC_0^{(k)}} LWC \quad (2)$$

where k is the cloud type. The constants $N_0^{(k)}$ and $LWC_0^{(k)}$ are listed in Tab. 1 for each cloud type. The extinction coefficient is computed as

$$\beta_{\text{RTTOV}} = N \tilde{\beta}^{(k)}, \quad (3)$$

where $\tilde{\beta}^{(k)}$ is a cloud type and satellite channel specific constant determining the extinction per particle.

Table 1: Effective droplet radius and the values for N_0 and LWC_0 for all RTTOV cloud types.

cloud type	$r_{\text{eff,w}}$ [μm]	N_0 [cm^{-3}]	LWC_0 [g cm^{-3}]
Stratus (continental)	7.33	250	0.28
Stratus (maritime)	11.29	80	0.30
Cumulus (continental clean)	5.77	400	0.26
Cumulus (continental polluted)	4.00	1300	0.30
Cumulus (maritime)	12.68	65	0.44

3.2 Input parameters for VISOP/MFASIS

Here one has to distinguish between the parameters required for the MFASIS method itself and the parameters required by VISOP to generate the MFASIS input parameters. Per column MFASIS requires at least 8 parameters: the total optical depths and mean effective particle radii for water and ice clouds, the albedo, the zenith angles of sun and satellite and the scattering angle. However, usually vertical profiles of the optical layer thickness, the effective radii and a vertical profile of the cloud cover will be specified. In this case MFASIS uses one of several available cloud overlap approaches (see Sect. 4.3) to generate a number of subcolumns or “streams” (not to be confused with the streams in discrete ordinate method) which represent the partial cloudiness in the column. For each subcolumn vertical integration yields the total optical depths and vertical averaging (weighted by the layer optical depth) is used to obtain the mean effective radii. Then the MFASIS interpolation is used to compute the reflectance for each subcolumn and the results are averaged.

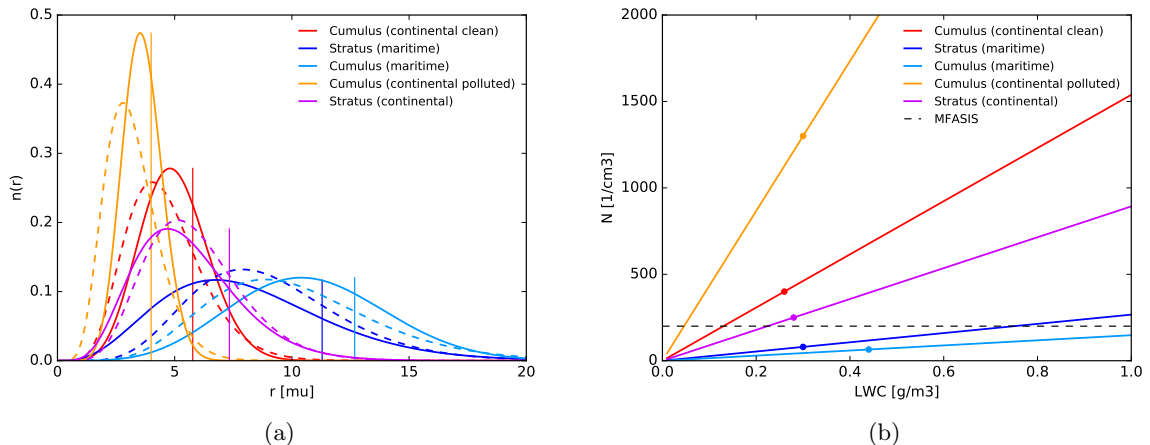


Figure 1: (a) Droplet size distributions $n_{\text{RTTOV},k}(r)$ of the 5 RTTOV clouds types (solid lines) and Gamma size distributions $n_{\Gamma,k}(r) \propto r^\alpha \exp^{-br}$ with $\alpha = 7$ (as used for the generation of the MFASIS LUT) resulting in the same effective radius $r_{\text{eff},w} = (\alpha + 3)/b$ as for the RTTOV distributions (dashed lines). All size distributions are normalized such that $\int_0^\infty n(r)dr = 1$. Thin vertical lines indicate the effective radius for each type. (b) Linear relations between droplet concentration N and liquid water content LWC assumed for the 5 RTTOV cloud types. Dots mark the value pairs (LWC_0, N_0) from Tab. 1. The black dashed line indicates the fixed value $N = 200\text{cm}^{-3}$ usually used in VISOP/MFASIS.

VISOP is responsible for computing the vertical profiles of effective radii and layer optical depths required by MFASIS from the model state. VISOP uses parameterizations to determine effective particle sizes for water and ice clouds. The effective droplet size parameterization by Martin et al. (1994) depends on the liquid water content LWC and a droplet concentration N , which in VISOP is usually kept constant at $N = 200\text{cm}^{-3}$. Examples of the relation between LWC and $r_{\text{eff},w}$ for different values of N are shown in Fig. 2. The effective ice particle size parameterization by Wyser (1998) depends on the ice water content IWC and the temperature. The water contents and effective sizes are then used to compute extinction coefficients and thus optical depths for each layer. For water clouds Eq. 13 in Hu and Stamnes (1993) defines a relation

$$\frac{\beta_{\text{VISOP}}}{LWC} = a_1 r_{\text{eff},w}^{b_1} + c_1, \quad (4)$$

where β_{VISOP} is the extinction coefficient and a_1 , b_1 and c_1 are tabulated for different wavelength and effective radius ranges in the paper. For ice clouds a similar relation by Fu (1996) is used.

3.3 A common set of input variables

Water clouds are treated quite differently in RTTOV-DOM and VISOP/MFASIS. RTTOV-DOM allows only for a finite number of effective radius values, whereas for VISOP/MFASIS the effective radius is a continuous input parameter. However, as will be demonstrated in Sect. 4, restricting VISOP/MFASIS to use only the RTTOV radii does not have a large impact on the satellite images. Also the different shapes of the size distributions will be shown not to have a significant impact. A more problematic difference is that N is assumed constant and $r_{\text{eff},w}$ is adjusted to fit to a given LWC in VISOP/MFASIS, whereas in RTTOV-DOM $r_{\text{eff},w}$ is assumed to be constant (for a given cloud type) and N is adjusted to fit to the specified

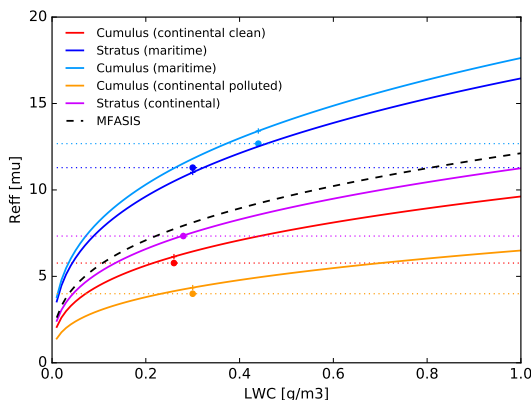


Figure 2: Relation between $r_{\text{eff,w}}$ and LWC' as proposed by Martin et al. (1994) for different values of N . For the colored lines the N values from Tab. 1 were used. For the black dashed line the value $N = 200\text{cm}^{-3}$ usually adopted in VISOP/MFASIS was used. The dashed horizontal lines indicate the effective radius values from Tab. 1 and the dots the corresponding LWC' values.

LWC . In other words, if the water content is reduced, RTTOV assumes that the droplets sizes do not change but some of the droplets evaporate. VISOP/MFASIS assumes that all droplets survive but shrink in radius. It is likely that in reality something in between these idealized processes will happen. For the typical values of LWC and N as from Table 1 the two approaches actually lead to very similar results – the Martin et al. (1994) parameterization nearly reproduces the $r_{\text{eff,w}}$ values from the table. For low values of LWC , however, more, smaller droplets and thus brighter clouds are generated by VISOP/MFASIS, in comparison to RTTOV-DOM.

A meaningful comparison of the two methods requires that a common set of input variables is used in a way that should lead to the same results if the radiative transfer approaches were equivalent. Here we follow the strategy to use VISOP as a wrapper around RTTOV-DOM so that for both methods only vertical profiles of LWC , IWC and cloud cover are required as input parameters. The effective ice particle diameter computed in VISOP with the parameterisation of Wyser (1998) can be used as input for both RTTOV-DOM and MFASIS. The $r_{\text{eff,w}}$ computed using Martin et al. (1994) have to be restricted to the RTTOV values (Tab. 1) so that they can serve as an input for both methods (for RTTOV by selecting the corresponding cloud type). To account for the different ways of computing the extinction coefficient from LWC , the input water content for RTTOV is modified by VISOP. It is set to a value

$$LWC' = \frac{\beta_{\text{VISOP}}}{\beta_{\text{RTTOV}}} LWC. \quad (5)$$

Within RTTOV-DOM the extinction coefficient is then computed according to Eqs. 2 and 3 as

$$\beta = \tilde{\beta}^{(k)} \frac{N_0^{(k)}}{LWC_0^{(k)}} LWC' = \beta_{\text{VISOP}}. \quad (6)$$

Therefore, RTTOV-DOM performs radiative transfer calculations for a water cloud with the same optical depth as MFASIS.

In principle, similar correction should be made to compensate for any difference in MFASIS and RTTOV-DOM concerning the way in which the extinction coefficient for ice clouds is computed from IWC . However, the required correction seems to be much smaller and could

not precisely diagnosed due to a numerical problem (see Sect. 4). Therefore, we refrained from investigating this problem at this point to concentrate on more important differences between RTTOV-DOM and MFASIS.

4 Differences in the radiative transfer

The common input variable strategy described in the previous section ensures that reflectance computations in RTTOV-DOM and MFASIS are performed for clouds with the same optical depths and the same effective particle radii. However, there are a number of differences in the radiative transfer processes that can lead to different results.

4.1 Water and ice clouds

As discussed already in Sect. 3, RTTOV-DOM and MFASIS assume by default different droplet size distributions. RTTOV is limited to 5 cloud types which are associated with fixed values of $r_{\text{eff,w}}$ and have different droplet size distribution shapes (see Tab. 1, Fig. 1). In MFASIS the droplet sizes are always characterized by a Gamma distribution and $r_{\text{eff,w}}$ is allowed to vary continuously between $2.5\mu\text{m}$ and $25\mu\text{m}$. To investigate the impact of these differences we computed reflectances for the idealized scenes used also in the generation of the MFASIS LUT (see Sect. 2), which consist only of two homogeneous clouds at fixed heights. For this problem any influence of the different treatments of the vertical structure or the cloud overlap in the two methods is excluded. Moreover, to allow for a clean comparison also the Rayleigh scattering and the absorption by trace gases was switched off. We considered two versions of RTTOV-DOM, one with the original size distribution functions (solid lines in Fig. 1) and one where the same Gamma distributions as in MFASIS were used (dashed lines in Fig. 1).

The results show that the different distribution functions have only very weak influence on the reflectance (compare green and blue lines in Fig. 3). This was to be expected, as Hu and Stamnes (1993) have shown that for a fixed effective radius the single scattering albedo, the symmetry factor and the extinction coefficient are insensitive to the shape of the distribution function. Moreover, Fig. 3 shows that in general MFASIS and RTTOV-DOM agree very well. Near the rainbow (local maxima in Fig. 3b) the reflectance deviations are somewhat larger but still limited to a few 10^{-2} . Significant differences can be seen for scattering angles larger than about 175° (marked with a thick black line in Fig. 3b), where reflectances are affected by the backscatter glory region. These scattering angles lie outside of the range considered in the MFASIS LUT generation and also RTTOV-DOM cannot be expected to produce reliable results here (see discussion in Scheck et al., 2016).

For ice clouds the same size distributions and optical properties are used in RTTOV-DOM and MFASIS (libRadtran option `baum_v36` with severely roughened aggregates, see Emde et al., 2016). As Fig. 4a shows, without the clear sky component the RTTOV-DOM reflectances are on average very similar but slightly smaller and show the same slope as a function of $r_{\text{eff,w}}$ as for MFASIS. However, the results are also affected by some form of numerical noise. The angular dependence of reflectance is again very similar for both methods (Fig. 4b). The noise problem prevents us from a precise comparison of RTTOV-DOM and MFASIS ice cloud reflectances here, but is not of practical relevance, as the noise vanishes when Rayleigh scattering is switched on (dark blue line in Fig. 4a). In this case an offset between the MFASIS and RTTOV-DOM reflectances can be observed, which is probably caused by a difference in the clear sky contributions to the reflectance (see next section).

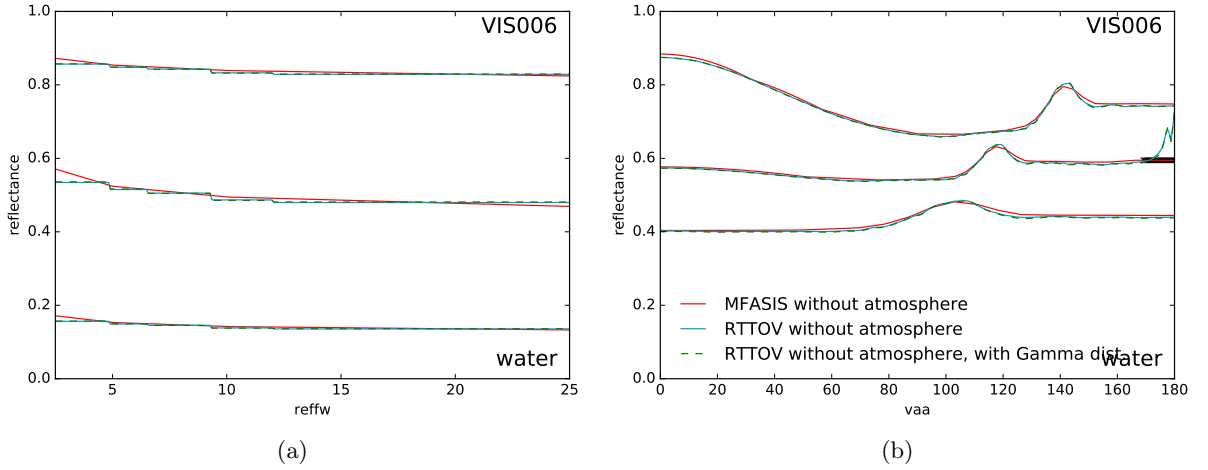


Figure 3: (a) Reflectance as a function of effective droplet radius for water clouds with optical depths $\tau_w = 100$, $\tau_w = 10$ and $\tau_w = 1$ (from top to bottom) computed using RTTOV-DOM and MFASIS for the $0.6\mu\text{m}$ SEVIRI channel. The RTTOV results were computed with the original size distributions and the same Gamma distribution as used in MFASIS. Rayleigh scattering and absorption by trace gases were switched off. The albedo is 0.1, $\theta_0 = 60^\circ$ and $\theta = 40^\circ$. (b) Reflectance as a function of the difference of the sun and satellite azimuth angles for different values of the solar zenith angle, $\theta_0 = 65^\circ$, $\theta_0 = 40^\circ$ and $\theta_0 = 15^\circ$ (from top to bottom). To avoid overlapping curves also the albedo was varied, it is 0.7, 0.3 and 0.0 (from top to bottom). The satellite zenith angle is $\theta = 40^\circ$ in all cases and $r_{\text{eff},w} = 11.3\mu\text{m}$. The thick black line indicates scattering angles larger than 171° , which are not part of the MFASIS table.

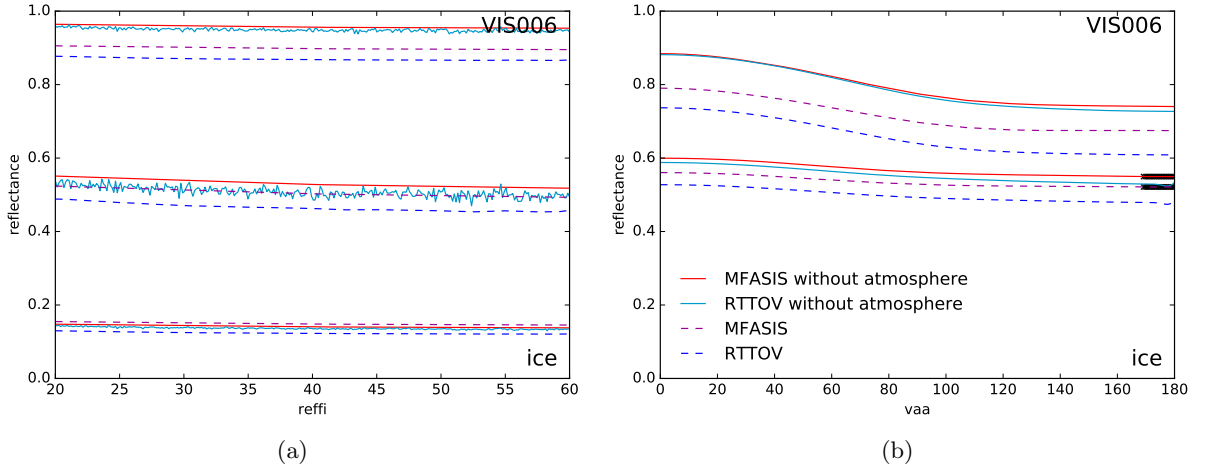


Figure 4: Like Fig. 3, but for ice clouds. In addition, RTTOV and MFASIS results including Rayleigh scattering and molecular absorption are included. Only results for $\theta_0 = 65^\circ$ and $\theta_0 = 40^\circ$ are shown in the right panel.

4.2 Clear sky contributions

Visible reflectances depend to first approximation on clouds and albedo. However, also Rayleigh scattering by and absorption by air molecules and trace gases² have some influ-

²And scattering and absorption by aerosol particles, which will not be discussed here.

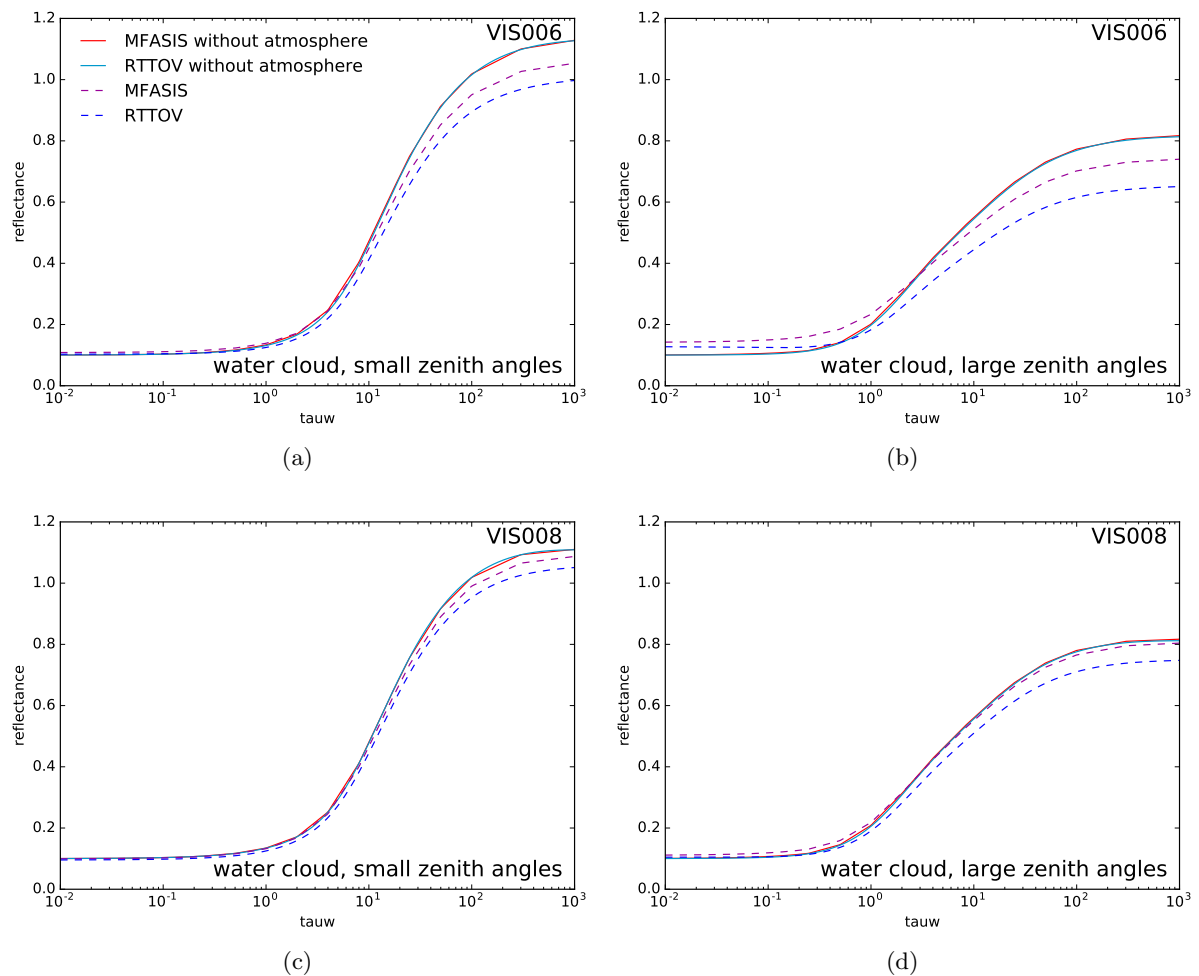


Figure 5: Reflectance as a function of water cloud optical depth for the $0.6\mu\text{m}$ (panels (a) and (b)) and $0.8\mu\text{m}$ (panels (c) and (d)) SEVIRI channels. In panels (a) and (c) the zenith angles are small, $\theta = 10^\circ$ and $\theta = 20^\circ$. In panels (b) and (d) they are relatively large, $\theta = 60^\circ$ and $\theta = 70^\circ$.

ence, in particular for large viewing angles, which maximize the optical path length in the clear sky atmosphere.

In the DOM implementation in libRadtran that has been used to compute the MFASIS LUT multiple scattering between all layers (cloudy and clear sky) is considered. To reduce the computational effort, RTTOV-DOM considers only multiple scattering between cloud layers and uses a single scattering approximation for the cloud free layers. Consequently, processes like the Rayleigh scattering of a photon from an air molecule and the subsequent scattering of the photon by a cloud towards the satellite (or the same in different order) are not accounted for in RTTOV-DOM. These processes are in many situations not very important, but as a comparison of MFASIS and RTTOV-DOM indicates, their influence is significant for dense, bright clouds. Figure 5 shows that reflectance as a function of the optical depth of the water cloud is very similar for MFASIS and RTTOV-DOM, when the clear sky contributions is switched off (curves labeled with “no atmosphere”). With Rayleigh scattering and molecular absorption the reflectance is reduced for thick clouds and slightly increased when no cloud is present. This effect is stronger in the $0.6\mu\text{m}$ channel (upper panels of Fig. 5) than in the $0.8\mu\text{m}$ channel (lower panels of Fig. 5), in accordance with the fact that the efficiency of

Rayleigh scattering increases strongly with decreasing wavelength. Moreover, reflectance is changed more strongly for large zenith angles (right panels) than small zenith angles (left panels), as expected from the clear sky path lengths that are increasing with the zenith angles. In all cases shown in Fig. 5 the RTTOV-DOM reflectances are significantly lower than the MFASIS reflectances for high optical depths, which can be attributed to the Rayleigh-cloud scattering processes that are included in MFASIS but missing in RTTOV-DOM.

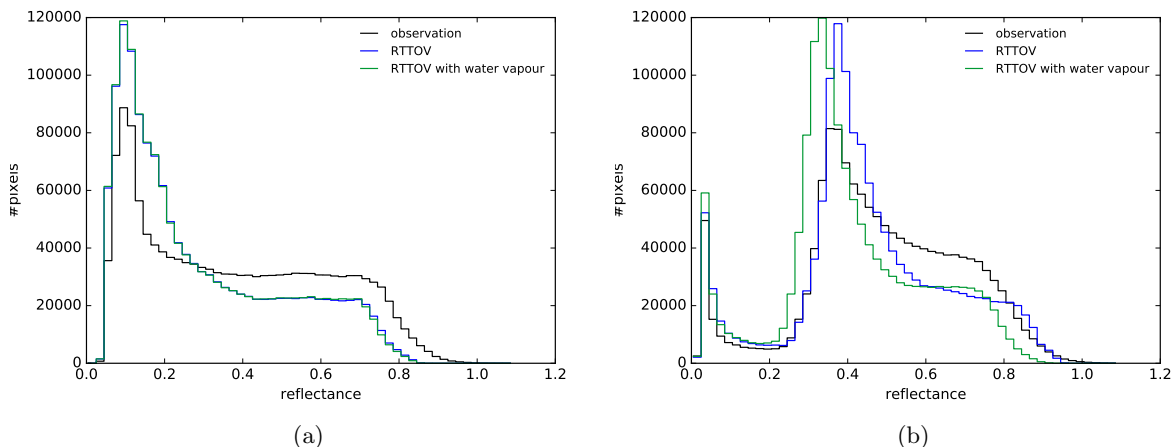


Figure 6: Reflectance histograms of RTTOV-DOM with and without accounting for water vapour for (a) the $0.6\mu\text{m}$ and (b) the $0.8\mu\text{m}$ SEVIRI channels for the full test period.

While Rayleigh scattering is weaker for the $0.8\mu\text{m}$ channel a second effect becomes important: absorption by water vapour. At the moment only a constant water vapour profile is assumed in MFASIS. For the RTTOV-DOM results discussed so far the same constant water vapour profile was used. To evaluate the importance of water vapour absorption we computed additional RTTOV-DOM satellite images for the test period. In the first series of images we used the varying water vapour profiles from the COSMO model states. In the second series the water vapour content was set to a very small value. The reflectance histograms for these two experiments are shown in Fig. 6 and indicate that for the $0.6\mu\text{m}$ SEVIRI channel the influence of water vapour can be neglected (Fig. 6a), while for the $0.8\mu\text{m}$ channel it is significant (Fig. 6b) and leads to a reduction of the reflectance of cloudy pixels by several 10^{-2} . For MFASIS varying water vapour content is thus a significant source of error for the $0.8\mu\text{m}$ channel and should be taken into account in future versions.

4.3 Cloud overlap

NWP and climate models cannot resolve clouds on scales smaller than their grid length. As the influence of these clouds is not negligible, the models rely on parameterization to take clouds on subgrid scales into account. These parameterizations generate additional cloud water content in cells where the grid scale cloud water content is zero but the relative humidity is higher than a height-dependent critical value, which is typically between 0.7 and 0.9. The cloud cover variable γ is smaller than one in these partially cloudy grid cells. As shown in Fig. 7a, without these subgrid clouds the cloud cover in the synthetic MFASIS satellite images for the test period is far too low. With the standard settings of the COSMO model the reflectance histogram is improved and with optimized subgrid settings that lead to more clouds the systematic error is reduced significantly (Fig. 7b). For comparison also

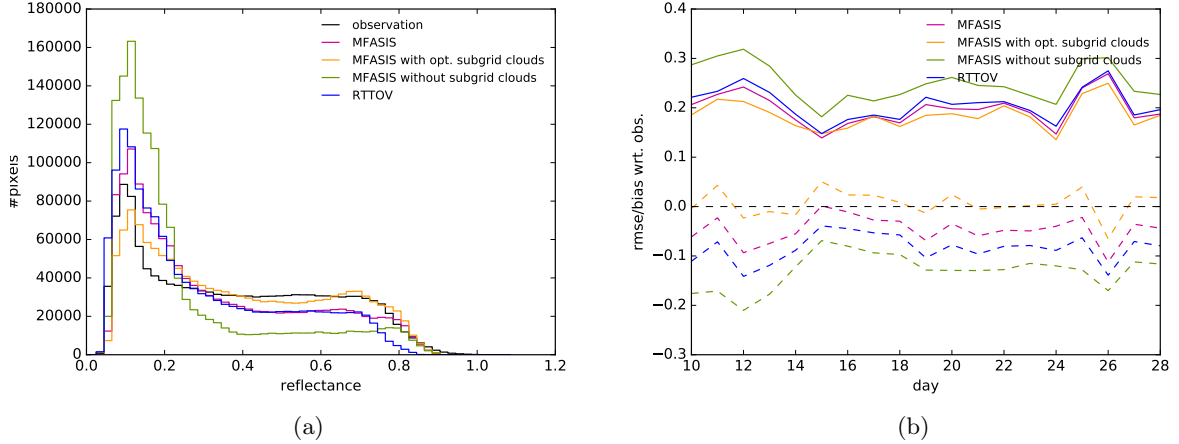


Figure 7: (a) $0.6\mu\text{m}$ reflectance histograms of RTTOV-DOM with and without atmosphere and MFASIS with and without optimized subgrid cloud settings and with effective radii restricted to the values of Tab. 1 for the test period. (b) Reflectance RMSE (solid) and bias (dashed) of the methods with respect to the SEVIRI observations.

the RTTOV results for the standard subgrid cloud settings are shown in Fig. 7, which are very similar to the MFASIS results except for the lower maximum reflectance caused by the Rayleigh-cloud scattering problem discussed in the previous section.

The fact that the partially cloudy grid cells are important implies that a further problem cannot be ignored. Whenever two or more partially cloudy cells are contained in a column of the computational grid, one has to make assumptions on how these subgrid clouds overlap. Changing these assumptions often does not have a large impact on the majority of pixels, but can have a strong impact on certain features in a satellite image. Moreover, taking these cloud overlap assumptions into account can lead to increased computational effort.

The simplest overlap assumptions are that the cloud overlap is either random or maximum. For maximum cloud overlap the total cloud cover of n layers with cloud cover γ_k is assumed to be

$$\gamma_{\text{tot}}^{\text{max}} = \max_{k=1,\dots,n} \gamma_k. \quad (7)$$

For two randomly overlapping clouds the probability to encounter at least one of them at a randomly chosen location is $\gamma_1 + \gamma_2 - \gamma_1\gamma_2$, which can be also written as $1 - \gamma_{\text{tot}}^{\text{rand}} = (1 - \gamma_1)(1 - \gamma_2)$ and generalized to n layers as

$$1 - \gamma_{\text{tot}}^{\text{rand}} = \prod_{k=1,\dots,n} (1 - \gamma_k). \quad (8)$$

An often used overlap assumption is random-maximum cloud overlap. Clouds in neighboring layers are assumed to follow the maximum overlap rule, whereas clouds separated by a cloud-free layer are assumed to overlap randomly. A formula approximating the mean total cloud overlap for this case is given by

$$1 - \gamma_{\text{tot}}^{\text{randmax}} = (1 - \gamma_1) \prod_{k=2,\dots,n} \frac{1 - \max(\gamma_k, \gamma_{k-1})}{1 - \gamma_{k-1}} \quad (9)$$

(Sundqvist et al., 1989). Examples for SEVIRI images computed with random-maximum and random cloud overlap are shown in Figs. 8a,b. A comparison with the difference plot Fig. 8c

indicates that the darkest and the brightest pixels do not depend strongly on the overlap assumption, whereas pixels with intermediate reflectance values are up to 50% brighter in the random overlap case.

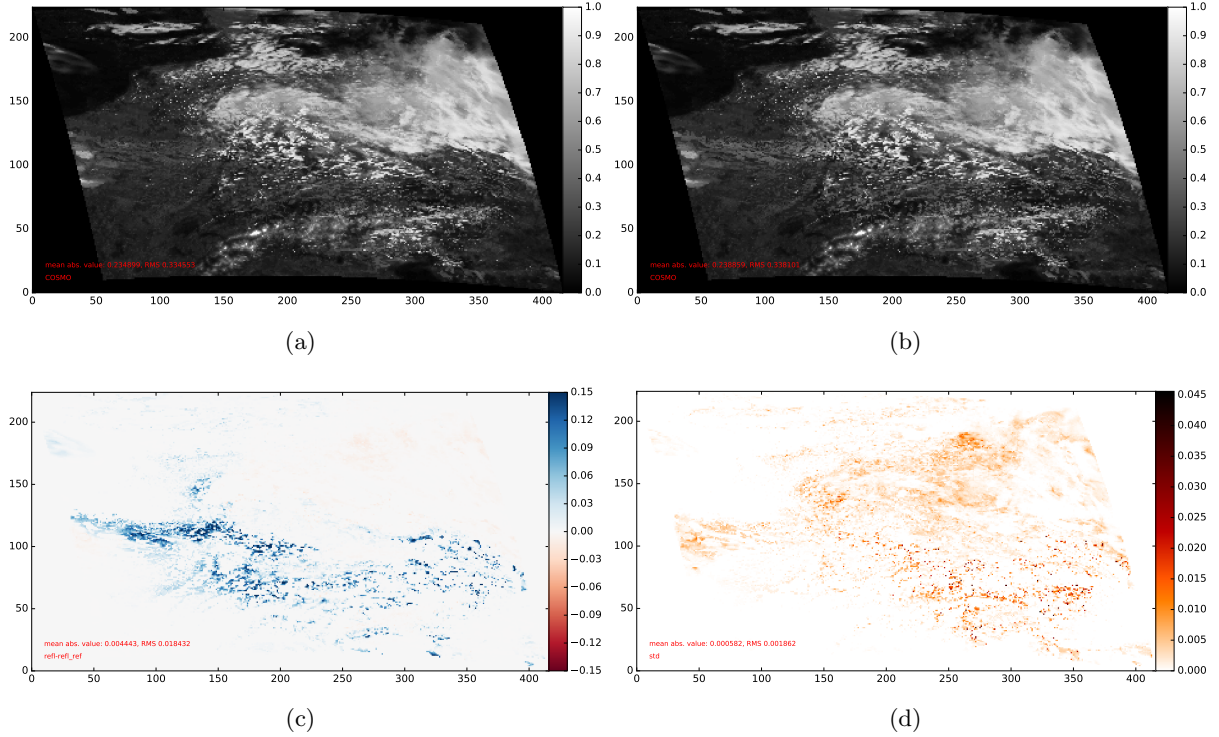


Figure 8: (a) Synthetic SEVIRI $0.6\mu\text{m}$ image for June 14th, 2012 computed with MFASIS and the random/maximum streams method with a variable number of streams. (b) Like (a), but using the random overlap assumption. (c) Difference between the images in (a) and (b). (d) Standard deviation of reflectance for an ensemble of 100 images computed with the stochastic overlap scheme using 128 subcolumns.

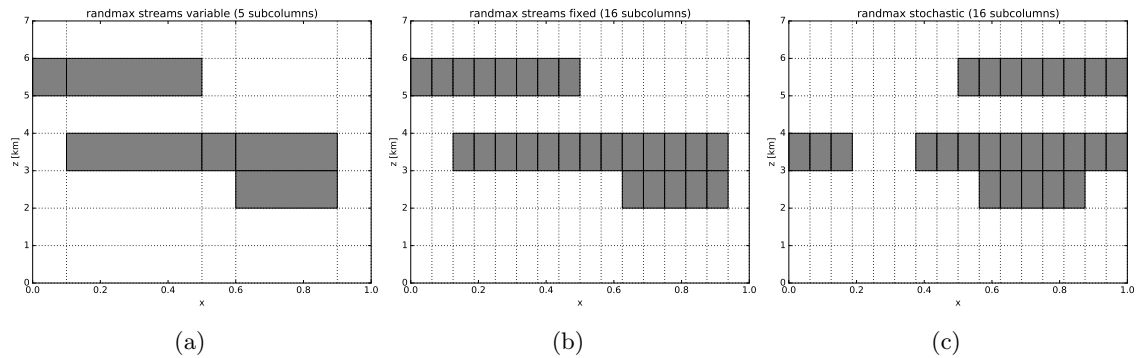


Figure 9: Random/maximum cloud overlap examples for a cloud layer between $z = 5\text{km}$ and $z = 6\text{km}$ with cloud cover 0.5 and two neighboring cloud layers between $z = 2\text{km}$ and $z = 4\text{km}$ with cloud covers 0.8 and 0.3. The cloud configuration assumed by the streams method is shown in panel (a), the discretized version with 16 subcolumns in panel (b) and one realization generated by the stochastic scheme in panel (c).

In the following we compare three different cloud overlap algorithms. To allow for a reasonable comparison between MFASIS and RTTOV results, Rayleigh scattering was always switched off (see Sect. 4.2) for the results discussed in the rest of this section. In the “streams” method (Matricardi, 2005) implemented in RTTOV and MFASIS, the total cloud cover is computed for each layer according to Eq. 9. Adopting a non-dimensional coordinate $x \in [0, 1]$ that spans the grid cell the cloud in layer k is assumed to extend from $x_k^L = \gamma_{\text{tot}} - \gamma_k$ to $x_k^R = \gamma_{\text{tot}}$. The grid cell is then divided into N “streams” or subcolumns such that every layer in every subcolumn is either completely cloud-covered or cloud-free. This process is illustrated in Fig. 9a and can lead to a rather high number of subcolumns to be considered. In the worst case $2n_z$ subcolumns have to be considered, where n_z is the number of model levels. The increased memory requirements associated with a high number of subcolumns is a disadvantage of the streams method.

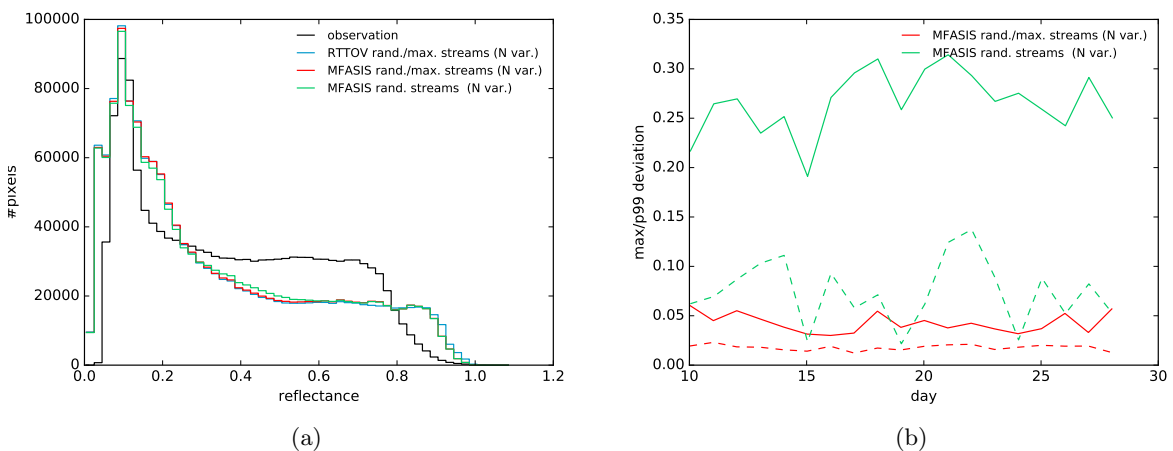


Figure 10: (a) Reflectance histogram of $0.6\mu\text{m}$ SEVIRI images for the test period computed using the random streams method in MFASIS and the random-maximum streams method in RTTOV-DOM and MFASIS. (b) Maximum deviation (solid lines) and 99% percentile of the deviation (dashed lines) of the random and random-maximum overlap MFASIS results with respect to the random-maximum overlap RTTOV-DOM results for each day of the test period.

The different implementations of the streams method in RTTOV-DOM and MFASIS seem to be equivalent, as results obtained for the random-maximum overlap assumption are very similar (Fig. 10). The reflectance histograms are nearly identical and the 99% percentile of the reflectance differences smaller than 10^{-2} . For comparison also random overlap MFASIS results are shown, which deviate much stronger from the random-maximum RTTOV results. The difference in the histograms (Fig. 10a) between random and random-maximum results appears to be quite small. However, this is a bit misleading as the reflectance can change quite significantly, but usually does so in only a small fraction of each satellite image (see the example in Fig. 8a-c).

As a potential alternative that avoids the problem of a high number of subcolumns in the streams method a discrete version of this approach was implemented in MFASIS. In the discrete version the subcolumns boundaries are located at fixed positions $\tilde{x}_i = i/N$ with $i = 0, 1, \dots, N$. The clouds are placed in these subcolumns following the same rules as in the original method, except that x_k^L and x_k^R are in each layer moved to the next smaller or larger \tilde{x}_i . To give an example, the discrete version of Fig. 9a is shown in Fig. 9b. To estimate how many discrete subcolumns are required, we compared the discretized version with the

original streams method for the June 2012 test period. As shown in Fig. 11a, using only two subcolumns leads to significant errors in the reflectance histogram. For larger numbers of subcolumns the error decreases strongly (Fig. 11b). For 16 subcolumns the 99% percentile reflectance error for all pixels and days is about 10^{-2} , which should be sufficiently low for most applications. For many purposes 4 or 8 subcolumns could also be acceptable. It should be noted here that the computational effort does not increase linearly with the number of subcolumns used for the discretization of the streams. Often several identical subcolumns will be generated by the overlap algorithm and can be merged before computing the reflectances. For instance, in the example shown in Fig. 9c there are only four different types of columns. In particular, all cloud-free subcolumns can be merged. Moreover, all the optical properties have to be computed only once per layer, not by layer and subcolumn. The computational effort of the discrete streams method could be significantly lower than for the original streams method.

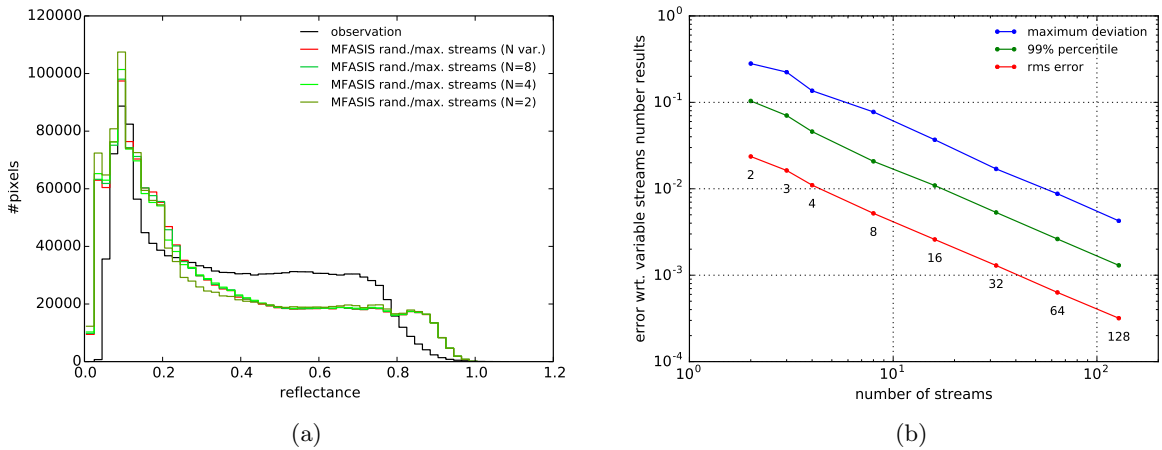


Figure 11: (a) Reflectance histogram of $0.6\mu\text{m}$ SEVIRI images generated by MFASIS for the test period using the original random-maximum streams method and the discrete version with 2, 4, and 8 streams. (b) Maximum deviation, 99% percentile of the deviation and root mean square deviation in reflectance of the discrete streams version with respect to the original streams version computed for the full test period as a function of the number of streams.

In addition to these deterministic cloud overlap schemes, which try to estimate the mean overlaps between cloudy layers averaged over all subgrid cloud realizations allowed according to the cloud overlap rules, a stochastic scheme is available in MFASIS. This scheme generates one random subgrid cloud realization compatible with the overlap rules. It uses the same subcolumn configuration as the deterministic scheme with the fixed number of subcolumns. However, clouds are placed into the subgrid cells according to non-deterministic rules. For the uppermost layer of a group of neighboring cloudy layers a random position is chosen, around which the cloud is centered. In the layers below clouds are placed randomly, but under the constraint that the overlap with the layers above (all layers of the same group, not just the layer directly above) is maximized. One realization for the example problem used above is shown in Fig. 9c.

The stochastic scheme allows for subgrid cloud configurations that are not considered in the streams method. For instance, the third cloudy layer does not overlap the first cloudy layer in the deterministic schemes (Fig. 9a,b), whereas for the stochastic scheme such an overlap is possible (Fig. 9c). There seems to be no physical reason why an overlap between the first and

the third cloudy layer should not be allowed. This example illustrates the limitations of Eq. 9, which does not take all possible cloud configurations into account. Given this limitations, one cannot expect the average reflectance for many cloud realizations generated by the stochastic scheme to converge exactly towards the reflectance computed by the deterministic scheme. However, a comparison of satellite images computed with the deterministic scheme and the stochastic scheme (using an ensemble of 100 different realizations) for the test period shows that in most cases the streams method is a good approximation. The RMS reflectance difference between the mean of the stochastic ensemble or one stochastic realization and the deterministic results is less than 10^{-2} for all days and the bias is very small (Fig. 12a). The difference is nearly the same for 16 and 128 subcolumns, indicating that the mean of the stochastic results does not fully converge towards the deterministic results. However, the 99% percentile difference between ensemble mean and deterministic results is only a few 10^{-2} and only for some outliers the difference reaches values of up to 0.3 (Fig. 12b).

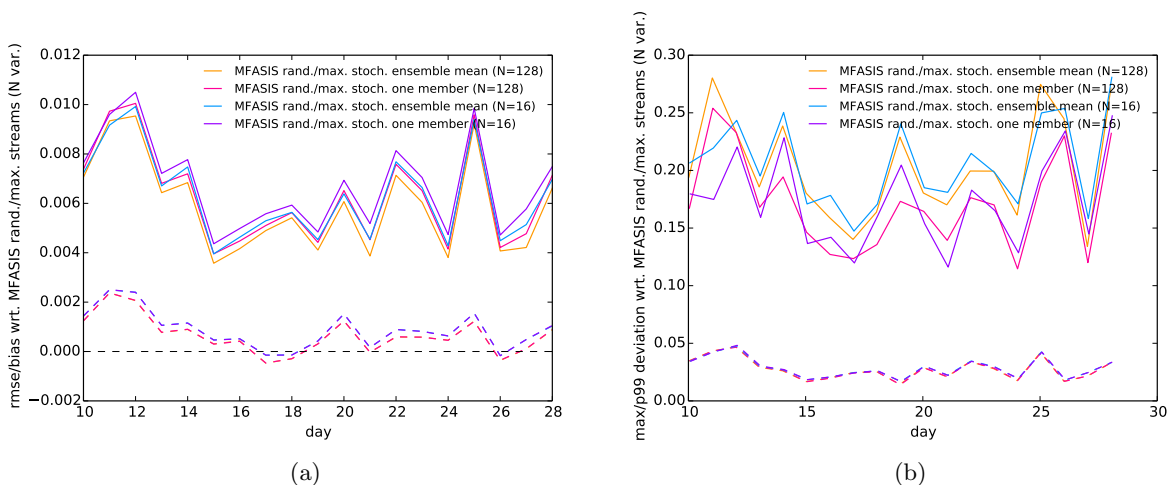


Figure 12: (a) Root mean squared deviation (solid) and bias (dashed) of the mean of 100 member satellite image ensembles computed with the discrete streams version using 16 and 128 subcolumns for each day of the test period. Also results for one member of each of the two ensembles are shown. (b) Like (a), but showing the 99% percentile (dashed) and the maximum (solid) deviation.

To decide how significant these differences are, one has to consider the spread, i.e. the ensemble standard deviation, of the stochastic version. An example for the reflectance spread in 100 realizations of the SEVIRI image for June 14th, 2012 using the stochastic random-maximum scheme is shown in Fig. 8d. The spread reaches values of several 10^{-2} and these values are not found only in pixels where the type of overlap matters (see Fig. 8c), but in a larger part of the image. Histograms of the ensemble spread and maximum-minimum reflectance for the full test period (Fig. 13a) show that for most pixels the reflectance is quite well-defined in the sense that the variation is much smaller than the mean value. Moreover, the difference in the mean value for 16 and 128 subcolumns is very small (Fig. 13b), suggesting that for most purposes it should be sufficient to use 16 or even less subcolumns in the stochastic scheme.

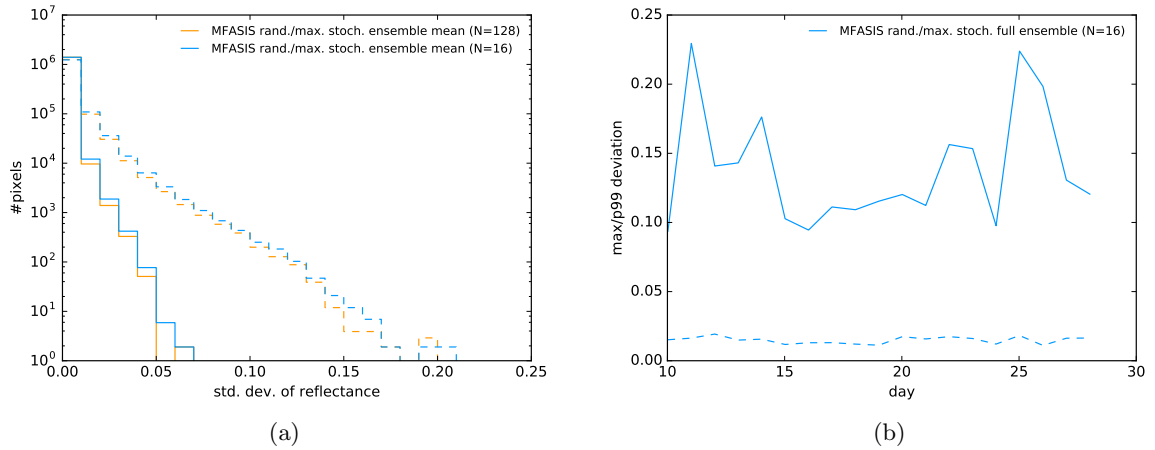


Figure 13: (a) Histogram of the ensemble spread of reflectance (solid) and the maximum-minimum reflectance in the ensemble (dashed) for the full test period. The stochastic random-maximum overlap approach with 128 subcolumns was used for an ensemble with 100 members. (b) Maximum deviation (solid) and 99% percentile of the deviation (dashed) between the mean ensemble reflectance values for 16 and 128 subcolumns.

5 Comparison using a RTTOV-generated MFASIS table

In the previous sections we discussed differences between RTTOV-DOM and a MFASIS version based on a LUT generated with the DOM implementation in libRadtran, which use the data on optical properties available in libRadtran. Here we compare RTTOV-DOM to MFASIS using a LUT generated by RTTOV-DOM itself. Thereby all differences related to optical properties and different assumptions in libRadtran and RTTOV are excluded. The MFASIS/RTTOV LUT was generated using an adapted version of a parallel Python script used to generate the MFASIS/libRadtran LUT, which took about 2 hours on 96 CPU cores.

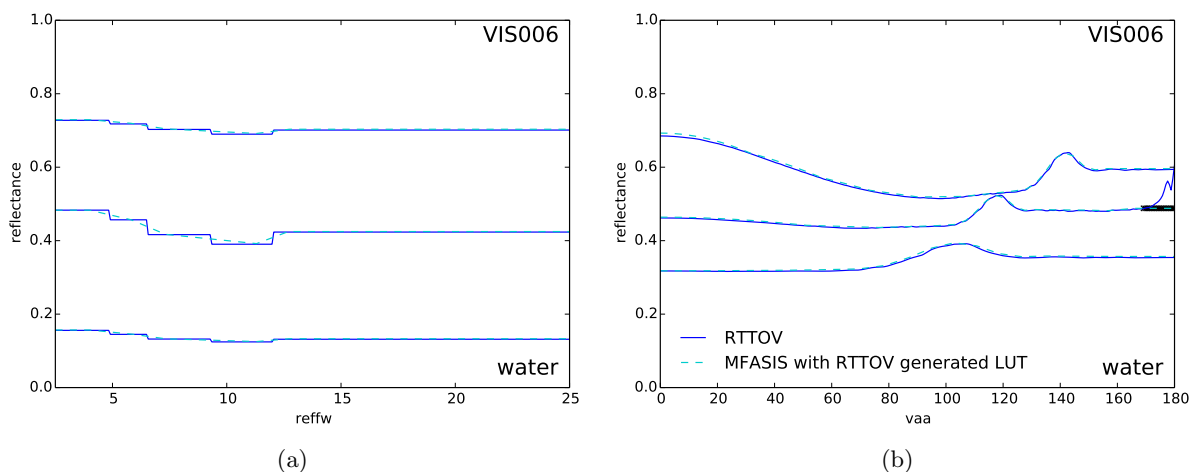


Figure 14: Like Fig. 3, but for RTTOV-DOM and MFASIS/RTTOV (including clear sky contributions).

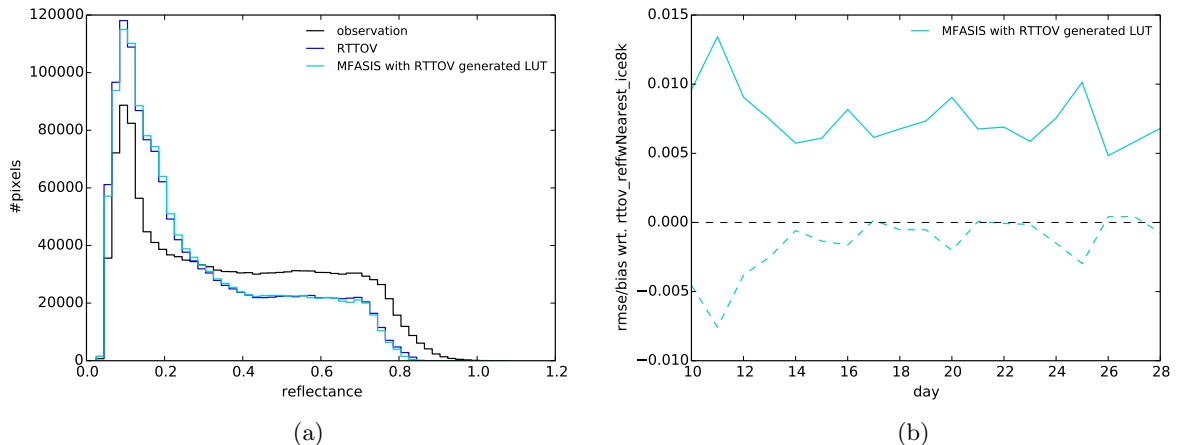


Figure 15: (a) $0.6\mu\text{m}$ reflectance histograms of RTTOV-DOM and MFASIS/RTTOV for the test period. (b) Reflectance RMSE (solid) and bias (dashed) of MFASIS/RTTOV with respect to RTTOV-DOM for all days of the test period.

The results are very similar to the comparison of DOM and MFASIS in Scheck et al. (2016). The reflectances computed by RTTOV are well approximated by MFASIS/RTTOV, except for scattering angles $> 171^\circ$ and $< 50^\circ$ that were not considered in the generation of the LUT (see Fig. 14 for examples). Also satellite images computed for the test period with the two methods are very similar (Fig. 15). The root mean squared reflectance error is about 0.07, as in Scheck et al. (2016). We did not perform a detailed analysis of all types of error as in Scheck et al. (2016), but it is to be expected that the same two types of error dominate here, that is the error related to the finite resolution of the LUT and the error caused by the simplification of compressing the vertical cloud structure into two homogeneous clouds (ice and water) at fixed heights.

6 Compatibility of MFASIS with the RTTOV framework

In this last part of the report we discuss if MFASIS could be included into RTTOV without changing the application programming interface (API) and which changes in the API could be useful for the users. As demonstrated in Sect. 3, the RTTOV input parameters are sufficient to define all input parameters for MFASIS. The effective ice particle size is an input parameter for both methods and the RTTOV input parameter cloud type determines the effective droplet radius required by MFASIS. For the results discussed in this report we used the parameterizations in VISOP to convert LWC to optical depth, but it would not be a problem to use instead RTTOV's approach to compute the optical depths. The impact of the different conversion method on the reflectance histogram for the test period is noticeable but not very strong (Fig. 16). As demonstrated in Sect. 4.1, for fixed optical depth the shape of the droplet size distribution does not make a significant difference for visible reflectances. Therefore, it is not necessary to take the size distribution shape into account when generating the MFASIS LUT. With the LUT computed with libRadtran MFASIS will generate slightly different results as RTTOV-DOM, owing to the different treatments of multiple scattering discussed in Sect. 4.2. For a LUT generated with RTTOV-DOM, the MFASIS results are very close to the RTTOV-DOM results for the $0.6\mu\text{m}$ channel (see Sect. 5), but the spatial

variation of water vapour will cause some differences for the $0.8\mu\text{m}$ channel (an upper limit for this effect is visible in Fig. 6). These differences will vanish when the treatment of multiple scattering is improved in RTTOV-DOM and the spatial variation of water vapour is taken into account in future versions of MFASIS.

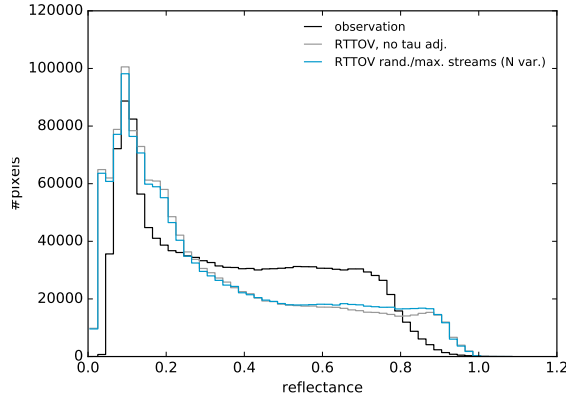


Figure 16: $0.6\mu\text{m}$ reflectance histograms of RTTOV-DOM results for the test period with the LWC to optical depth conversion methods of RTTOV (gray) and VISOP (blue). Rayleigh scattering was switched off for this comparison.

Although it would be possible to include MFASIS in RTTOV without any changes in the API, two changes would be useful. Firstly, one could introduce additional cloud type values to indicate that the conversion from LWC to optical depth should make use of the nonlinear relations used in VISOP instead of the linear relations defined for the five cloud types in RTTOV. Secondly, one could allow the user to directly specify the effective droplet radius, in the same way the effective ice particle diameter can be specified already in the current RTTOV version. This would be particularly useful for NWP models with a two-moment microphysics scheme where prognostic values for the effective radii can be derived.

7 Conclusions

In the course of a six week visiting scientist mission we compared two methods to generate synthetic visible satellite images, RTTOV-DOM and MFASIS. The main results of the comparison are:

- For clouds MFASIS and RTTOV-DOM generate similar reflectance results.
- Some differences exist in the less important clear sky contributions.
- Different cloud overlap schemes do not cause strong differences in the results.
- MFASIS could be used as a fast emulator for RTTOV-DOM.

Several recommendations for improvements in RTTOV and MFASIS based on the comparison results can be summarised as follows:

- The treatment of multiple scattering in RTTOV-DOM should be improved.
- The treatment of water vapour absorption should be improved in MFASIS, taking into account humidity profiles from the model state.
- RTTOV users should be given a way to specify the effective cloud droplet radius.

References

- Michael Baldauf, Axel Seifert, Jochen Frstner, Detlev Majewski, Matthias Raschendorfer, and Thorsten Reinhardt. Operational convective-scale numerical weather prediction with the cosmo model: Description and sensitivities. *Monthly Weather Review*, 139(12):3887–3905, 2011. doi: 10.1175/MWR-D-10-05013.1.
- S. Chandrasekhar. *Radiative transfer*. 1960.
- C. Emde, R. Buras-Schnell, A. Kylling, B. Mayer, J. Gasteiger, U. Hamann, J. Kylling, B. Richter, C. Pause, T. Dowling, and L. Bugliaro. The libradtran software package for radiative transfer calculations (version 2.0.1). *Geoscientific Model Development*, 9(5):1647–1672, 2016. doi: 10.5194/gmd-9-1647-2016. URL <http://www.geosci-model-dev.net/9/1647/2016/>.
- Qiang Fu. An accurate parameterization of the solar radiative properties of cirrus clouds for climate models. *Journal of Climate*, 9(9):2058–2082, 1996. doi: 10.1175/1520-0442(1996)009<2058:AAPOTS>2.0.CO;2.
- Y. X. Hu and K. Stamnes. An accurate parameterization of the radiative properties of water clouds suitable for use in climate models. *Journal of Climate*, 6(4):728–742, 1993. doi: 10.1175/1520-0442(1993)006<0728:AAPOTR>2.0.CO;2.
- G. M. Martin, D. W. Johnson, and A. Spice. The measurement and parameterization of effective radius of droplets in warm stratocumulus clouds. *Journal of the Atmospheric Sciences*, 51(13):1823–1842, 1994. doi: 10.1175/1520-0469(1994)051<1823:TMAPOE>2.0.CO;2.
- M. Matricardi. The inclusion of aerosols and clouds in rtiasi, the ecmwf fast radiative transfer model for the infrared atmospheric sounding interferometer. Shinfield Park, Reading, July 2005. Corrected version posted on December 2012.
- Mayer, B. and Kylling, A. Technical note: The libRadtran software package for radiative transfer calculations - description and examples of use. *Atmospheric Chemistry & Physics*, 5:1855–1877, July 2005.
- Leonhard Scheck, Pascal Frèrebeau, Robert Buras-Schnell, and Bernhard Mayer. A fast radiative transfer method for the simulation of visible satellite imagery. *Journal of Quantitative Spectroscopy and Radiative Transfer*, 175:54–67, 2016.
- Stamnes, K., Tsay, S.-C., Jayaweera, K., and Wiscombe, W. Numerically stable algorithm for discrete-ordinate-method radiative transfer in multiple scattering and emitting layered media. *Journal of Applied Optics*, 27:2502–2509, June 1988. doi: 10.1364/AO.27.002502.
- Hilding Sundqvist, Erik Berge, and Jon Egill Kristjansson. Condensation and cloud parameterization studies with a mesoscale numerical weather prediction model. *Monthly Weather Review*, 117(8):1641–1657, 1989. doi: 10.1175/1520-0493(1989)117<1641:CACPSW>2.0.CO;2.
- Klaus Wyser. The effective radius in ice clouds. *Journal of Climate*, 11(7):1793–1802, 1998. doi: 10.1175/1520-0442(1998)011<1793:TERIIC>2.0.CO;2.